

Author's Accepted Manuscript

Tensile characterization of a lead alloy: creep induced strain rate sensitivity

Luigi M. Viespoli, Audun Johanson, Antonio Alvaro, Bård Nyhus, Alberto Sommacal, Filippo Berto



PII: S0921-5093(18)31718-0
DOI: <https://doi.org/10.1016/j.msea.2018.12.039>
Reference: MSA37311

To appear in: *Materials Science & Engineering A*

Received date: 6 September 2018
Revised date: 23 October 2018
Accepted date: 10 December 2018

Cite this article as: Luigi M. Viespoli, Audun Johanson, Antonio Alvaro, Bård Nyhus, Alberto Sommacal and Filippo Berto, Tensile characterization of a lead alloy: creep induced strain rate sensitivity, *Materials Science & Engineering A*, <https://doi.org/10.1016/j.msea.2018.12.039>

This is a PDF file of an unedited manuscript that has been accepted for publication. As a service to our customers we are providing this early version of the manuscript. The manuscript will undergo copyediting, typesetting, and review of the resulting galley proof before it is published in its final citable form. Please note that during the production process errors may be discovered which could affect the content, and all legal disclaimers that apply to the journal pertain.

Tensile characterization of a lead alloy: creep induced strain rate sensitivity

Luigi M. Viespoli^{a1}, Audun Johanson^b, Antonio Alvaro^c, Bård Nyhus^c, Alberto Sommacal^{a,b,c}, Filippo Berto^a

^aDepartment of Mechanical and Industrial Engineering, Norwegian University of Science and Technology (NTNU), Norway

^bNexans Norway, Innspurten 9, 0663 Oslo, Norway

^cSintef Industry, Richard Birkelands vei 2B, 7031, Trondheim, NORWAY

luigimv@stud.ntnu.no

Abstract

The aim of this work is to investigate and define the tensile properties of cable sheathing lead alloy. In particular its strain rate sensitivity due to the pronounced creep already present at room temperature, in relation to the material work hardening and processing is object of study. Therefore, a series of specimens have been manufactured using cable sheathing of three different extrusion thicknesses and tested in displacement control at different strain rates. The practical difficulties generated by the highly plastic behavior have been overcome by the use of Digital Image Correlation (DIC) technique as a tool for measuring the strain field on the specimen surface. The creep behavior has been described, modeled and calibrated using Isight and finally implemented in the FEA code Abaqus. Two different numerical models have been used for modelling the time dependent deformation, a power law and the Anand model. The first predict correctly the response of the alloy in the primary creep region while the second shows better results for secondary creep.

Keywords: creep, plasticity, digital image correlation, finite element analysis, lead, microstructure

Introduction

Lead alloys used in subsea cable sheathing are usually associated with a low melting point T_m , i.e. about 590 K, and therefore a high relative operation temperature, around $0.5 T_m$, even at room temperature. At this temperature, time dependents phenomena including creep, relaxation and recrystallization have a significant influence on the mechanical properties of the material. The time dependent mechanisms, which imply a strain rate dependency on the monotonic tensile properties, must therefore be accounted for in order to accurately predict the mechanical behavior of components manufactured from lead alloys, such as power cable sheathing or battery grids. These responses are due to the influence of the active creep mechanisms also at low stress levels; particularly the apparent variation of the elastic modulus both in function of temperature and strain rate has been studied both for lead and lead-free solders. In the case of pure polycrystalline metal lattices, the size of the grain has an influence on the creep response, with an increase of strain rate for a given stress in the presence of smaller grains, due to a greater contribution of boundary sliding. A similar influence has been detected and reported on the yield stress. On the specific topic of the characterization of the mechanical properties of lead alloys used for the production of subsea cable sheathing, some studies have been conducted. Feltham investigated the mechanisms of creep deformation for lead alloys focusing on the influence of the grain size and intragranular substructure. Its conclusion is that the dislocation movement activation energy is a function of the volume self-diffusion, of the stress and, through a parameter q , of the Burgers' vector and of the average distance between dislocations. q is found independent of the applied stress and satisfactory results were obtained

¹ Richard Birkelands vei 2B, Trondheim, Norway

in the assumption of an exponential correlation of q with the temperature. Sahota et al. performed compressive tests on work hardened commercially pure and on three different lead alloys, investigating the influence of alloying elements such as copper, antimony and tellurium on the secondary creep strain rate. Harvard tested several different lead alloys with the aim of categorizing them for the proper use in the different power cables. Dollins and Betzer synthesized the results of an extensive testing campaign of lead alloys for cable sheathing focusing also on the influence of the production process on the long term creep behavior. Anelli et al. conducted fatigue testing on lead alloy E, slightly supersaturated Pb-Sb alloy. Their tests at different strain amplitude and rate have found a limited influence of temperature and grain size on the fatigue life of a properly manufactured cable.

Material and metallurgical investigation

Lead alloy of composition according to Table 1 was extruded into a pipe of 82 mm outer diameter (OD) and 1.1, 1.8 and 3.3 mm thickness during the cable production process. The choice of the alloy object of the study is driven by the necessity of working on a real sub-sea power cable sheathing material. Due to the slow operational cycles undergone by the cables generated by oceanic currents, tides and thermal expansion, it is important to understand the influence of the strain rate on the stress level induced in the cable. The cables have been cut, the pipes unfolded, then the specimens have been machined to a flat dog-bone geometry, figure 5. During the flattening procedure, the same strain rate has been applied according to the different thickness.

Table 1. Test material composition.

Pb [wt%]	Sb [wt %]	Sn [wt %]
99.3	0.2	0.5

For the understanding and characterization of the alloy's properties, it is important to understand the microstructure of the sheathing and its influence on the stress-strain response. With careful procedure, due to the extreme thermal and mechanical sensitivity of the alloy, a series of samples for metallographic investigation have been prepared. They have been cut from the non-tested sheathing in as-manufactured condition. The planes along which the investigation has been performed are indicated as A and B in figure 1. The grain size has been measured with the average grain intercept technique and the results are summarized in table 2. Figure 4 shows the result of the investigation in the two planes for the three specimens at a magnification of 200x.

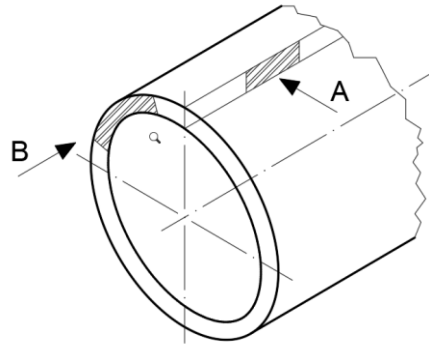


Fig 1. Scheme of the planes adopted for the metallography.

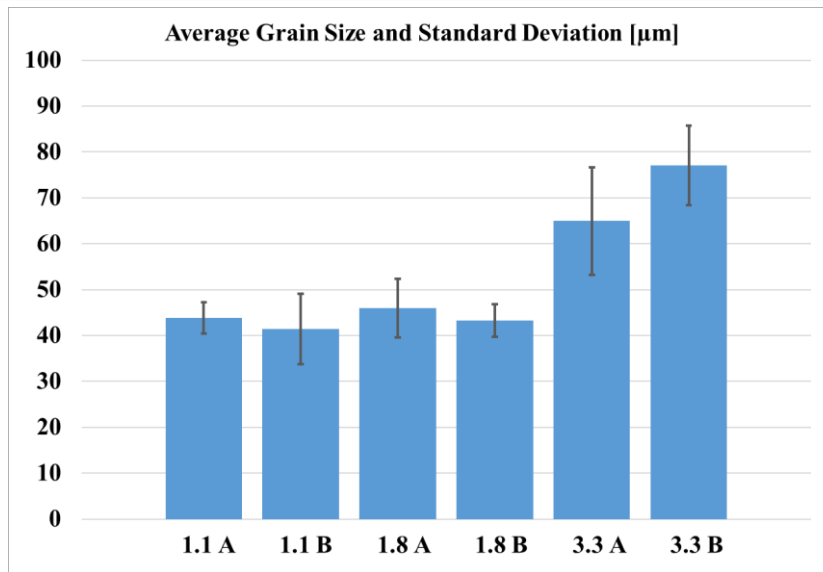
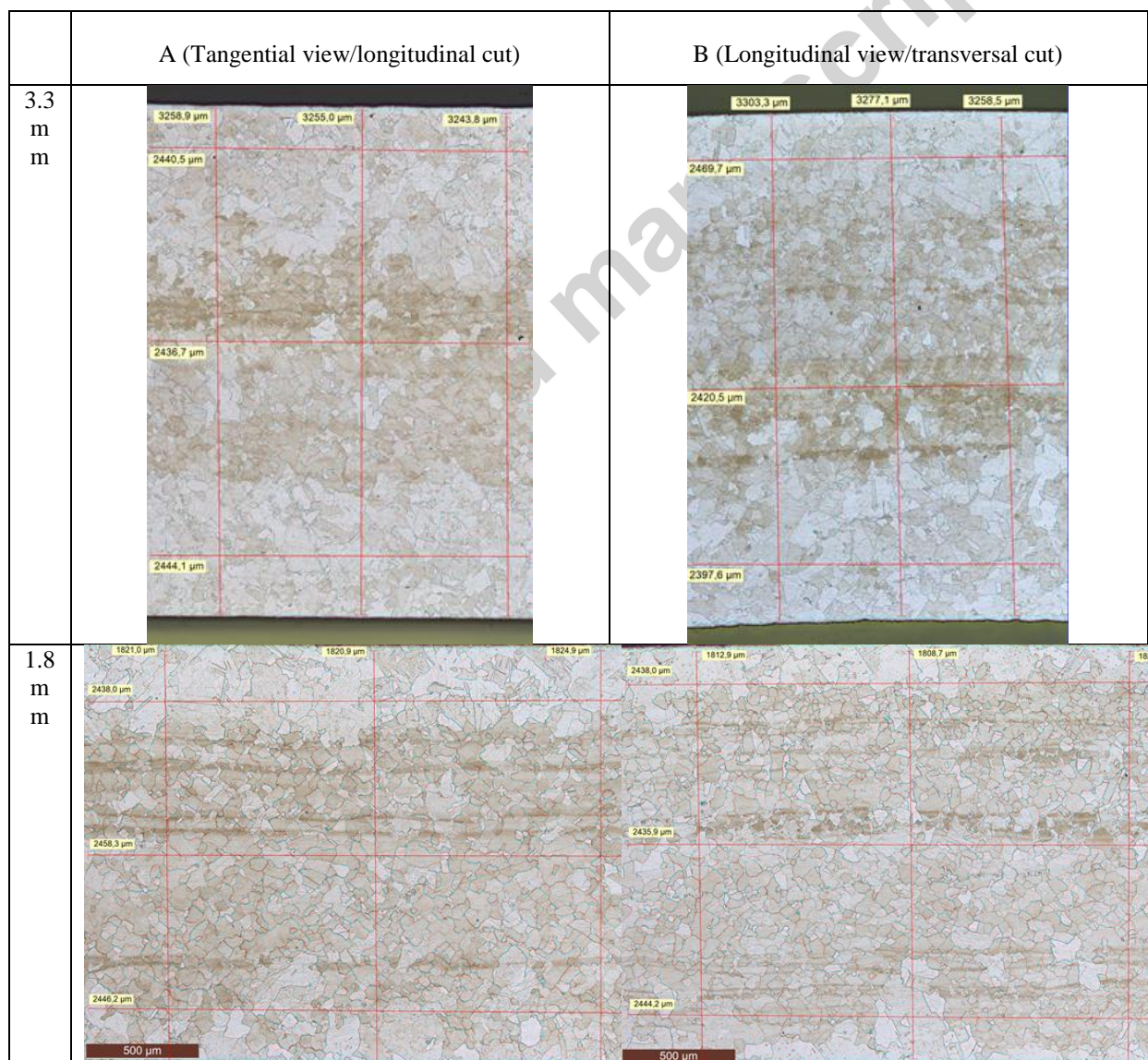


Fig 2. Average Grain Intercept synthetic results according to thickness and grinding plane, see figure 3, 50x.

Table 2. Average Grain Intercept extended results, see figure 3, 50x

Extrusion thickness [mm]	Plane orientation (see figure 1)	Line	Line length [μm]	Grain boundaries count	Average grain size on line [μm]
1.1	A	1	2428	51	47.6
		2	2423	52	46.6
		3	2421	63	38.4
		4	1026	24	42.8
		5	1026	22	46.7
		6	1024	25	41.0
	B	1	2452	43	57.0
		2	2448	56	43.7
		3	2432	60	40.5
		4	1094	29	37.7
		5	1055	31	34.0
		6	1037	29	35.7
1.8	A	1	2438	47	51.9
		2	2458	44	55.9
		3	2446	56	43.7
		4	1821	50	36.4
		5	1821	40	45.5
		6	1825	43	42.4
	B	1	2438	55	44.3
		2	2436	54	45.1
		3	2444	53	46.1
		4	1813	42	43.2

		5	1809	40	45.2
		6	1821	51	35.7
3.3	A	1	2440	41	59.5
		2	2438	41	59.4
		3	2444	27	90.5
		4	3259	51	63.9
		5	3255	59	55.2
		6	3244	53	61.2
	B	1	2470	28	88.2
2		2421	37	65.4	
3		2398	30	79.9	
4		3303	38	86.9	
5		3277	48	68.2	
6		3259	44	74.1	



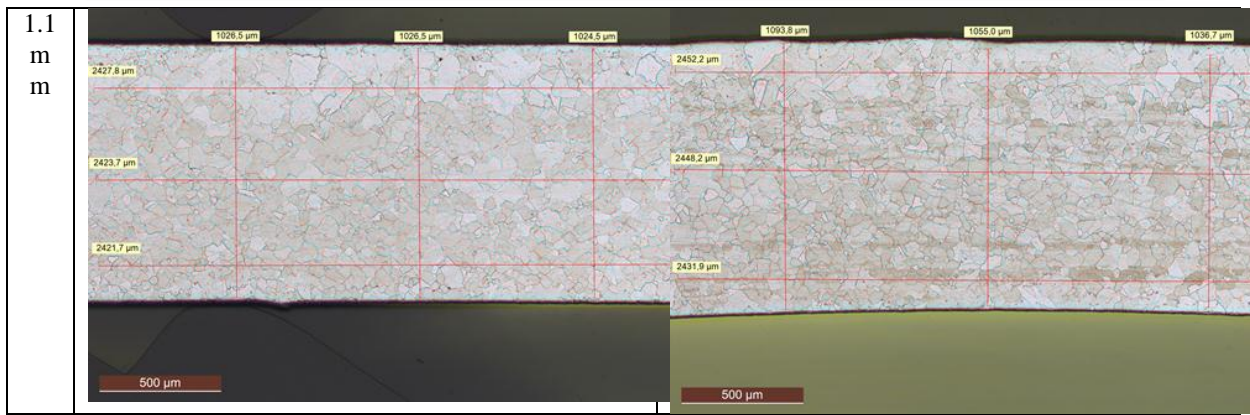
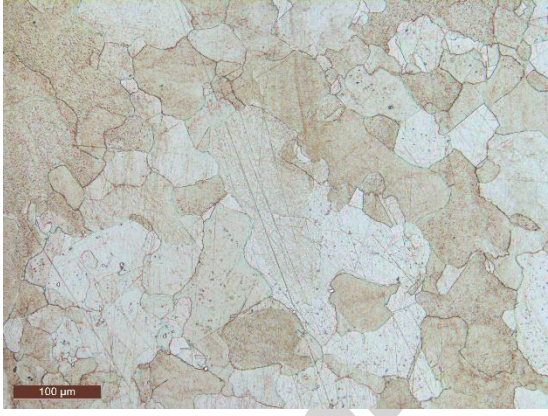
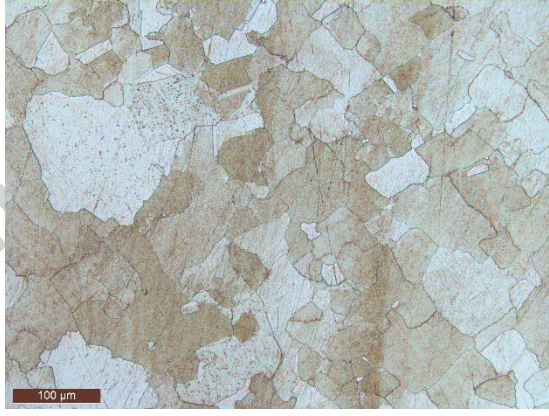

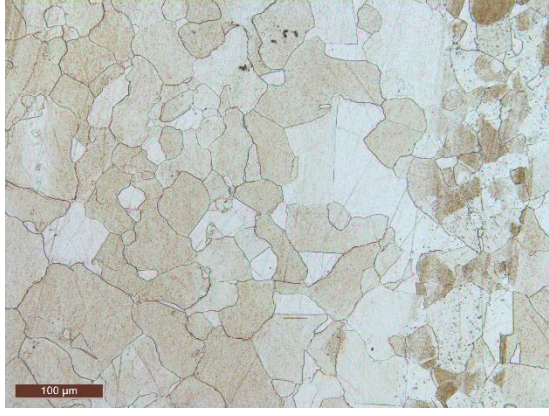


Fig 3. Synthesis of the Average Grain Intercept measurements reported in table 2 according to figure 1 grinding plane, 50x.

	A (Tangential view/longitudinal cut)	B (Longitudinal view/transversal cut)
3.3 mm		
1.8 mm		

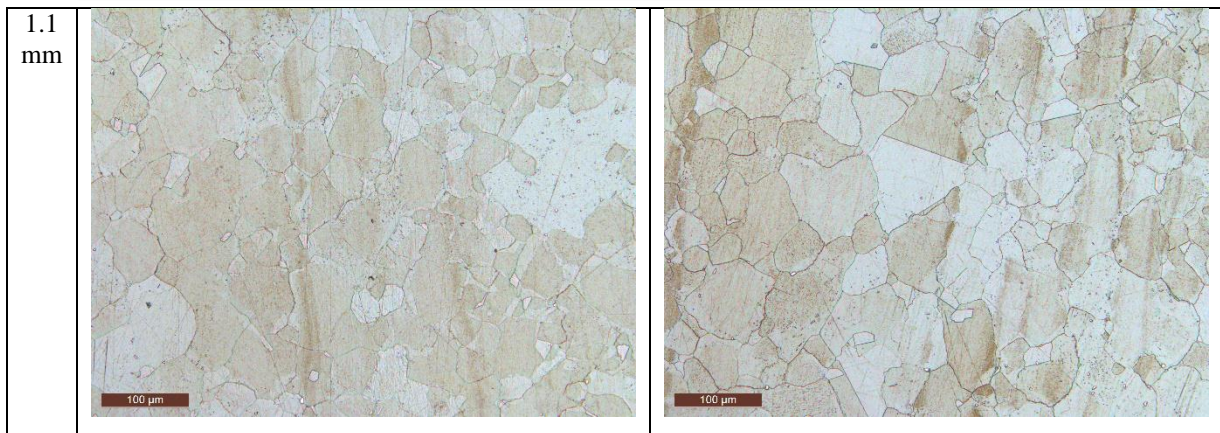


Fig 4. Detail of the grain structure according to figure 1 grinding plane, 200x.

According to the results of the AGI, in table 2, the average grain size for the 1.1 and 1.8 mm extrusion thickness is very similar, around $43 \mu\text{m}$, while the 3.3 mm extrusion thickness leads to a bigger grain size, around $70 \mu\text{m}$. This has a major influence in the creep behavior and material's mechanical response, as shown in the following paragraph. During the polishing process it is possible that small localized plastic deformations are induced in the material, like surface scratching. This originates small grains, which are not indicative of the true structure of the sheathing. These grains have been discarded from the statistical computation. Differentiating the results of the AGI on the A plane, no systematic difference of the grain size in the longitudinal and radial direction is seen for the 1.1 and 1.8 mm thick specimens, while a slight difference, with the grains on average 17.7% longer in the longitudinal direction, is present for the 3.3 mm thick samples. This indicates that the recrystallization of the sheathing at room temperature after the manufacturing removes the grain elongation induced by the extrusion.

Tensile testing procedure

The aim of the paper is to provide a material model of the alloy adopted able to reproduce its mechanical response to deformations imposed at room temperature and suitable for integration in finite element component modelling. In order to collect the necessary data, a series of tests on tensile specimens has been executed. The tensile specimens have been cut from lead sheathings of three different thicknesses and tested at room temperature at different strain rates. To enhance the precision of the numerical models, their correctness has then been verified with respect to the results from a relaxation test. During the testing the material has shown primary and secondary creep behavior, with the latter reached for the slower strain rate tests. The behavior observed is characterized by an influence of the strain rate both on the stress level and on the apparent elastic modulus. Since all the test have been performed at room temperature, no temperature dependence is accounted for. Moreover, the thicker specimens, 3.3 mm, have shown a higher stress response compared to the 1.8 and 1.1 mm thick ones. The results presented consist in a series of static tests performed at different strain rates on specimens of different thicknesses, whose design and dimensions are reported in Figure 5a. The nominal strain rate imposed to the specimens during the test, ranging from $1\text{E-}7 \text{ 1/s}$ to $1\text{E-}3 \text{ 1/s}$, is computed over the free length, that is, the constant width section of the specimen. The tests have been recorded via a Prosilica GC 2450 digital camera and the frames used have been then used for DIC analysis of the field of deformation in the plane using the eCorr DIC post-processor. The strain adopted as reference, to approximate the material behavior, is the infinitesimal strain in the longitudinal direction, computed on a vector in the central section of the specimen, as indicated by a white line in fig. 5b.

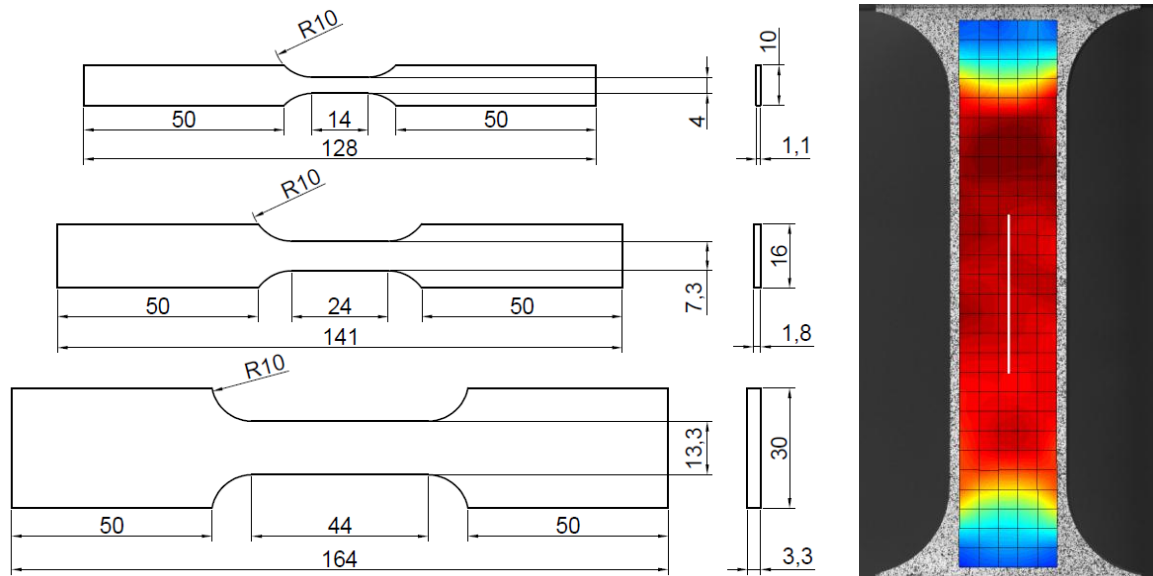
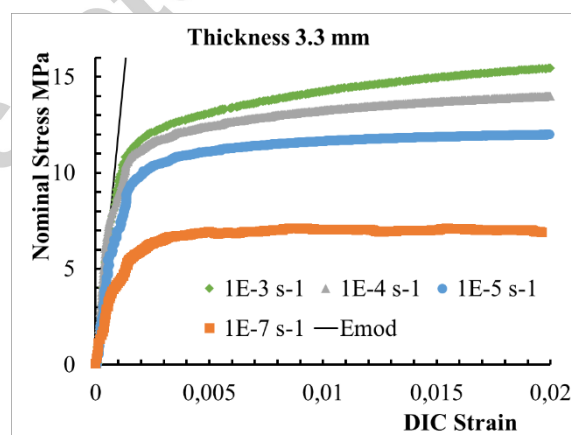


Fig 5. a) Specimens geometries and dimensions. b) An example of the DIC mesh and longitudinal strain field: the white line represents the vector adopted for the quantification of the strain.

The extremely low stresses at which the alloy shows plastic behavior, united with the presence of room temperature viscous flowing, originate practical difficulties in performing the tensile testing. In particular, the border effects due to the deformation of the specimen under the pressure of the clamping system, makes impossible to accurately estimate the strain imposed to the material simply by utilizing the clamp stroke. Therefore, the adoption of the DIC technique has permitted to investigate the behavior of the material, numerically reconstructing the in-plane strain field on the specimen's surface.

Tensile testing results

The results, summarized in figures 6 and 7, indicate that two major factors influence the tensile response of the material: the thickness and the strain rate. As the strain rate is reduced, so it is the load necessary in order to reach a given strain level indicating a pronounced viscous behavior of lead alloy, even at room temperature. The first sensible influence can be as the strain rate is lowered from $1E-3$ to $1E-4$ $1/s$ of strain rate and the loss in maximum stress is enhanced as the testing strain rate is further lowered. The second variable that clearly affect the material tensile properties is the sample thickness: contrarily to what is common seen for metals, the thicker is specimens, the higher is the resistance in terms of nominal stress.



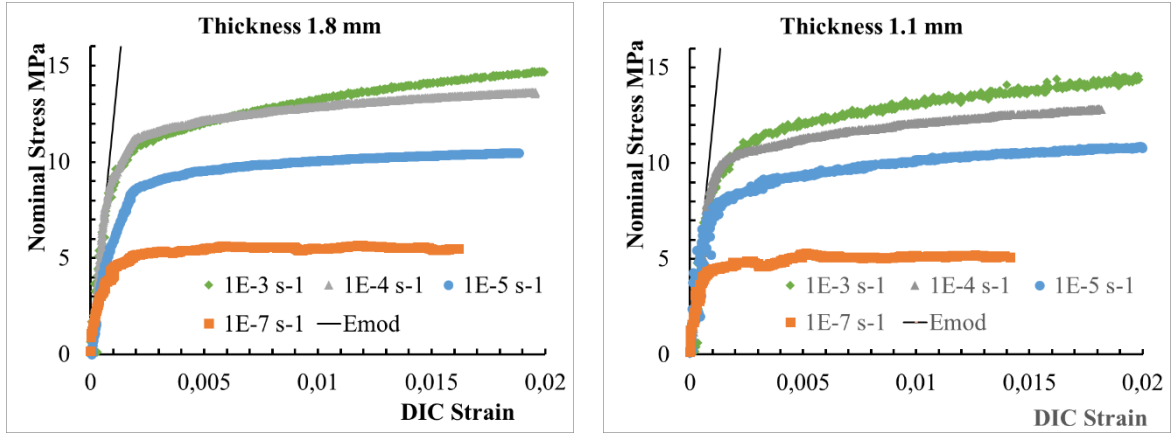


Fig 6. Comparison of the Digital Image Correlations results grouped for thickness.

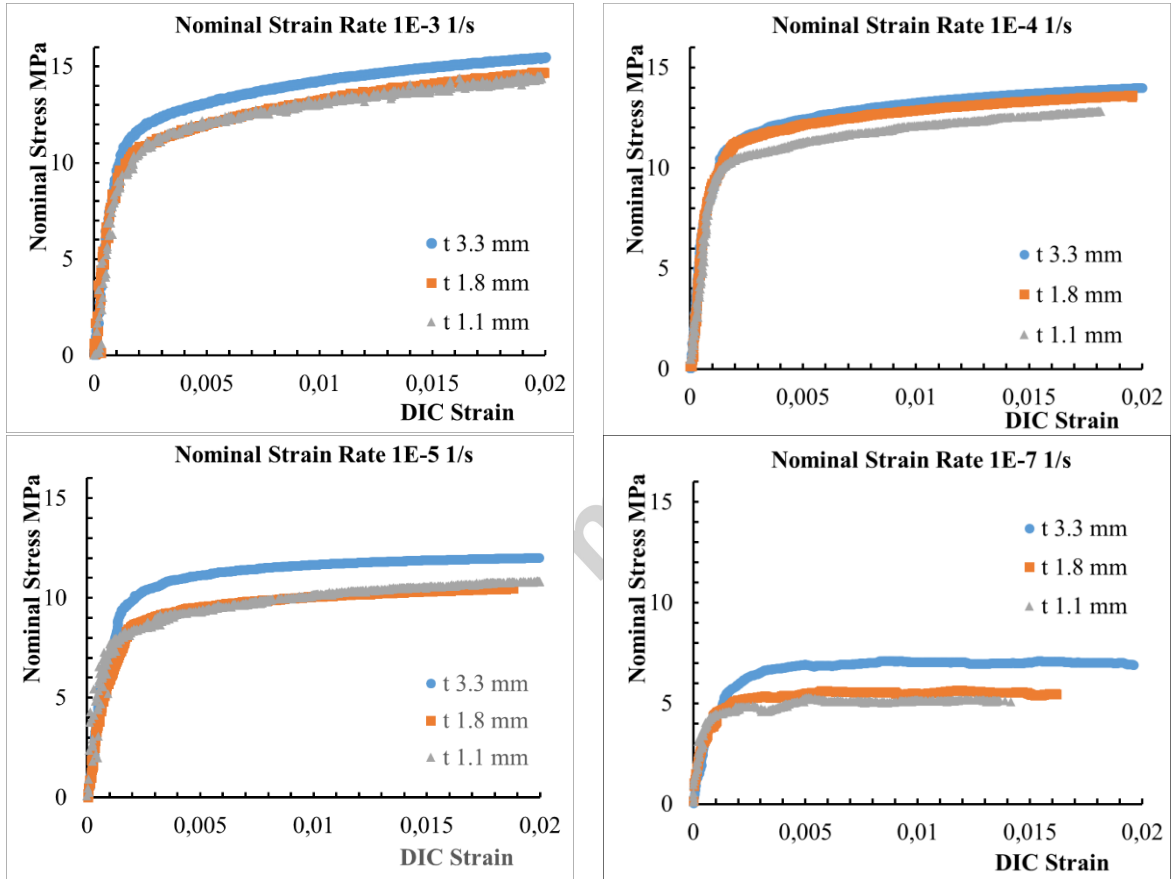


Fig 7. Comparison of the Digital Image Correlations results grouped for nominal strain rate.

Strain rate sensitivity of the young's modulus

By observing the initial stress-strain response of the material, and determining the Young's modulus as the slope of the curve, it has been experimentally observed a decrease of this value as strain rate is reduced. This trend is consistent with respect to previous works on Lead and Lead-free solder alloy, among those Motalab et al. , Pradeep et al. , Pang et al., who showed a linear dependence between the elastic modulus and both temperature and strain rate. Furthermore, they implemented the Anand model to numerically replicate the experimental result. Pang et al. studied the behaviour of a 63Sn/37Pb solder alloy for different temperature and strain-rate values, suggesting the following equation:

$$E(T, \dot{\epsilon}) = (a_3 T + a_2) \log(\dot{\epsilon}) + (a_1 T + a_0) \quad (1)$$

Pang's equation shows a good agreement with experimental data, since no temperature dependent test were conducted, only the strain rate dependent variables were computed. The result for 3.3 and 1.8 mm thick specimens are shown in figure 8.

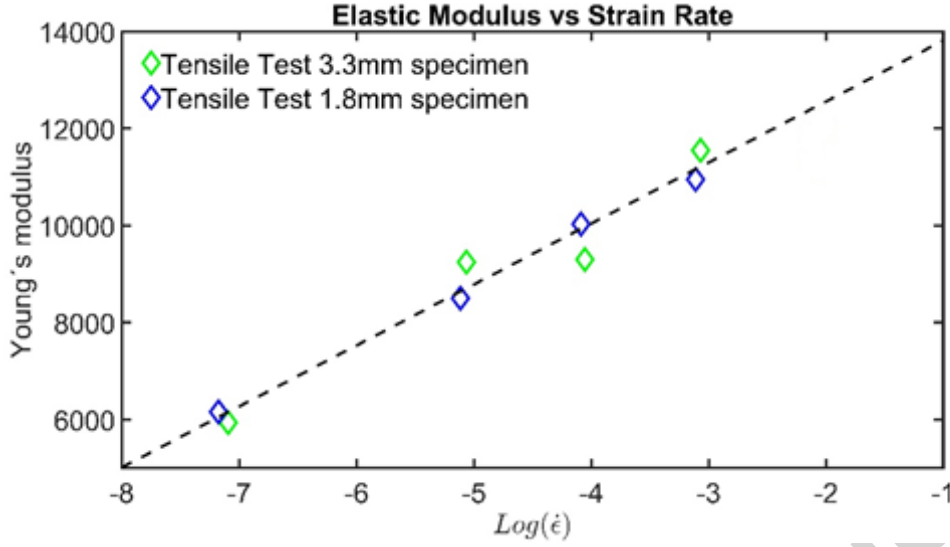


Fig 8. Variation of the apparent elasticity modulus as a function of the strain rate.

With, lacking data on the influence of the temperature:

- $(a_3 T + a_2) = 1257 \text{ MPa}$
- $(a_1 T + a_0) = 15070 \text{ MPa}$

It is possible to implement this result in the calibration of the material, adopting a user sub-routine which modifies the elastic modulus according to the strain rate at the previous iteration. It must be stressed that this is an engineering approach and does not correspond to the physics of the phenomenon. Although this procedure improves the capability of the models implemented in the following paragraphs to describe the initial part of the loading, the results of the calibration presented are at constant elastic modulus, in order to investigate their capability to deal with the problem as they are provided.

Power Law creep model

A model to reproduce the mechanical response of the alloy to a deformation imposed has been tested using FEA in Abaqus environment. After having defined elastic and plastic behavior, the time dependent strain component has been defined as a power law, using the preset strain hardening form :

$$\dot{\epsilon}^{cr} = (A\tilde{\sigma}^n [(m+1)\epsilon^{cr}]^m)^{\frac{1}{m+1}} \quad (2)$$

Where:

$\dot{\epsilon}^{cr}$ is the uniaxial equivalent creep strain rate, $\sqrt{\frac{2}{3}} \dot{\epsilon}^{cr}$; $\dot{\epsilon}^{cr}$

$\tilde{\sigma}$ is the uniaxial equivalent deviatoric stress,

A , n and m are to be calibrated to reproduce the right creep behavior. For a physically meaningful solution, A and n have to be positive and $-1 < m \leq 0$. In the Isight loop, figure 9, the three tensile simulations have been run simultaneously. Experimental and numerical response are compared after each calibration cycle in the data matching component with respect to two different quantities: the absolute difference between the experimental and simulation curves and the maximum absolute value. In such way both a global and local fit of the data is guaranteed.

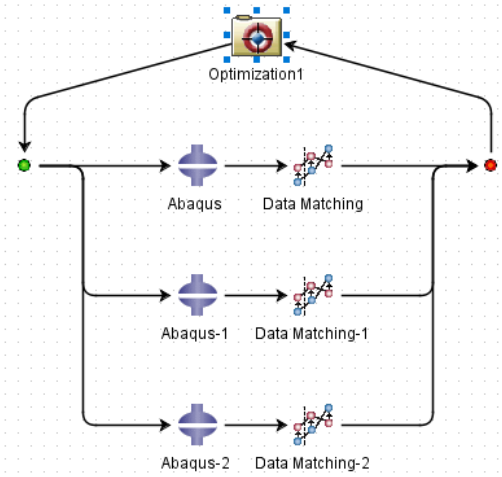


Fig 9. Optimization loop set in Isight for the calibration of the creep constants.

The model parameters as fitted are listed in Table 3,4. Table 3 summarizes the elasticity modulus, Poisson ratio and the three parameters of the power law model fitted with the aid of Isight. In table 4, the plastic curves for the material ideally in absence of creep are reported. These are individuated as a material response slightly stronger than the response at a nominal strain rate of $10E-3$ s⁻¹. This is a reasonable approach considering that the influence of the viscous deformation is very limited for the two highest strain rates tested and yields to fairly accurate results in the calibration of the creep models, as shown in figure 10. The same parameters are adopted, for the sake of uniformity, in the calibration of the Anand creep model in the next paragraph. The model adopted is feasible for the description of primary creep behavior. The secondary creep is characterized by a constant creep strain rate for a given stress level. The tests are executed at constant strain rate and a plateau is observed in the Stress-Strain curve for the tests at a nominal strain rate of $1E-7$ 1/s. This indicates that these tests lasted long enough so that the material entered the secondary creep phase, thus making the model unfit for the scope. This can be clearly seen in Figure 10, where the slope of the numerical stress-strain curve at the nominal strain rate of $1E-7$ 1/s is always greater than zero, giving a poor fitting for the slowest deformation.

Table 3. Power law model constants as fitted for power law model.

Thickness [mm]	E [MPa]	ν	A	n	m
1.1 – 1.8	12000	0.431	7.27818E-10	5.10577	-0.389647
3.3	12000	0.431	5.27817E-10	5.22075	-0.468147

Table 4. Plastic table adopted for power law and Anand model calibration.

Thickness [mm]			
1.1 – 1.8		3.3	
σ [MPa]	ϵ_{pl}	σ [MPa]	ϵ_{pl}
7.0	0.0	7.4	0.0
7.6	8.46e-05	7.9	6,00E-05
7.9	0.000134662	8.45	0.00013
8.5	0.000256403	9.05	0.00021

9.1	0.000418085	9.8	0.00031
9.8	0.000636959	10.5	0.00044
10.45	0.000935883	10.95	0.00057
10.8	0.00112436	11.3	0.00068
11.45	0.00166643	11.6	0.0008
11.8	0.00215645	11.8	0.00093
12.3	0.00337669	12.05	0.00108
12.8	0.0049784	12.26	0.00129
13.4	0.00703124	12.55	0.00158
13.7	0.00821398	12.9	0.00198
14.6	0.0125104	13.15	0.0024
15.5	0.0182811	13.47	0.0031
15.8	0.0205588	13.95	0.0042
16.4	0.0261663	14.3	0.0052
16.7	0.0301544	14.6	0.0064
17.3	0.0438478	14.9	0.0075
17.9	0.0719805	15.25	0.0088
18.5	0.122769	15.65	0.011
18.8	0.157931	16.6	0.0173
19.4	0.244784	17.3	0.0248
20.0	1.0	20.0	1.0

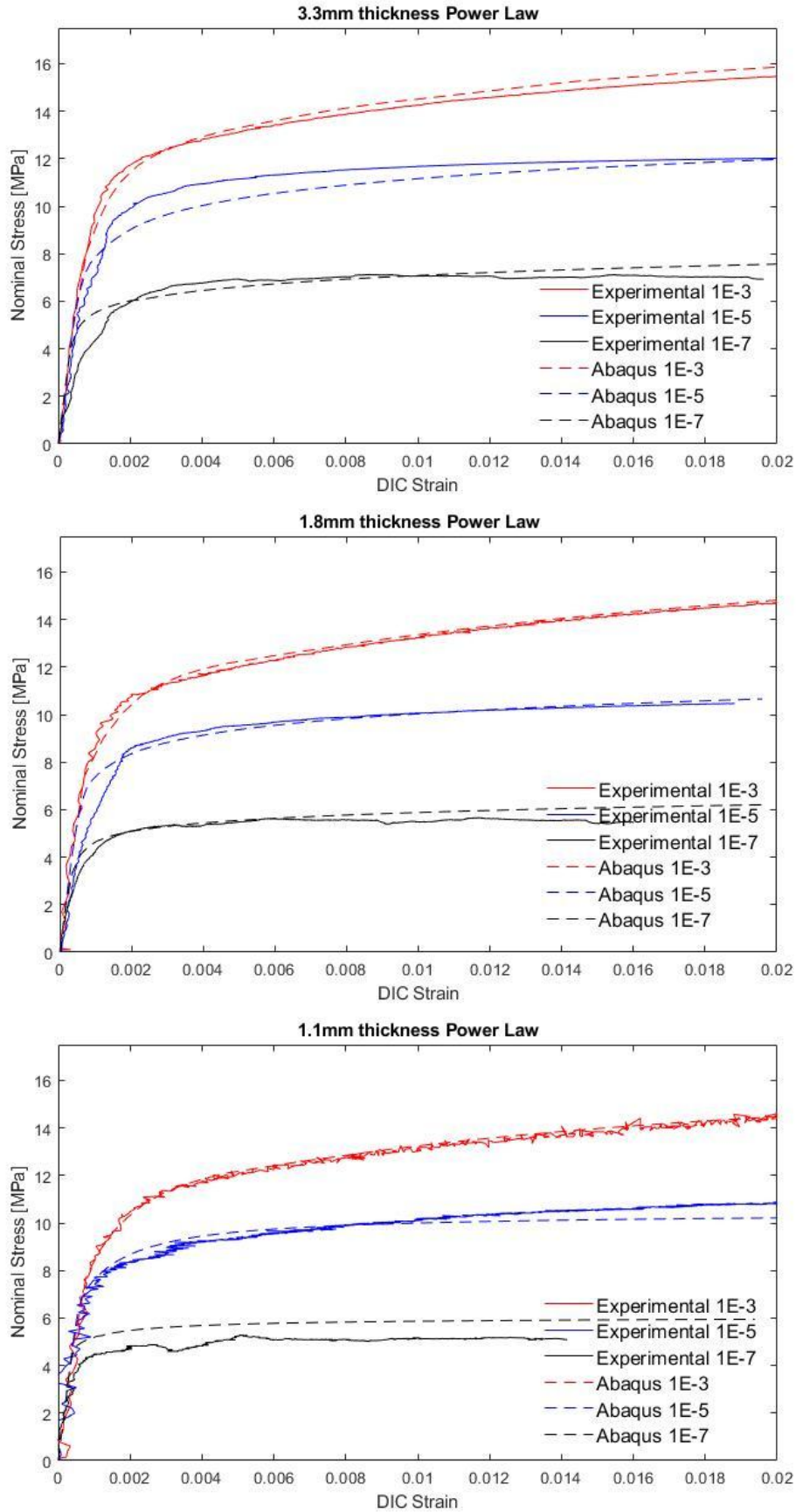


Fig 10. Power law model fitting compared with experimental results for three different strain rates.

Anand creep model

The model utilized describe both primary and secondary creep was initially proposed by Anand, et al. - for predict the rate-dependent deformations of metal in the high temperature range. Although it was originally developed to describe hot-working processes, it shows great result in predicting creep behavior for a wide range of alloys, mainly in the electronics field. In the microelectronics industry is commonly used to predict and verify the reliability of solders exposed to thermal cycling, and the necessary model constants are available in literature for a large number of materials. The model constitutive equation considers both strain hardening and temperature dependent behavior and it has been showing good predicting ability with respect to primary and secondary stage creep transition. The Anand model implemented in Abaqus presents fifteen parameters, six more with respect to the model proposed by Anand et al . A comparison between the original and Abaqus version of the model is reported in , with the latter showing a more precise fitting of experimental response for a wide range of temperature. The relation between stress and strain rate is model by the flow equation:

$$\dot{\epsilon}^{cr} = A * \exp\left(-\frac{Q}{R(\theta - \theta^z)}\right) \left[\sinh\left(\frac{\xi \bar{q}}{s}\right)\right]^{\frac{1}{m}} \quad (3)$$

Where:

- A is called “pre-exponential factor”
- Q is the activation energy
- m is the strain rate sensitivity exponent
- R is the universal gas constant
- ξ is a material parameter
- θ^z is the absolute value of the temperature
- \bar{q} , $\dot{\epsilon}^{cr}$ are defined above

Equation (3) is equal, except for the term s , to Garofalo's equation (4), that is commonly used for modelling the relationship between steady state stress and steady state creep strain .

$$\dot{\epsilon}_{ss}^{cr} = A * \exp\left(-\frac{Q}{R(\theta)}\right) [\sinh(\xi \sigma_{ss})]^{\frac{1}{m}} \quad (4)$$

The internal structure of the material is characterized by an internal variable, s . This has the dimension of a stress and represent the isotropic resistance opposed by the material to plastic flow. The evolution equation considers dynamic process such as strain hardening and recovery:

$$\dot{s} = h_0 \left|1 - \frac{s}{s^*}\right|^a \text{sign}\left(1 - \frac{s}{s^*}\right) \dot{\epsilon}^{cr} \quad (5)$$

with

$$s^* = \hat{s} \left[\frac{\dot{\epsilon}^{cr}}{A} \exp\left(\frac{Q}{R(\theta - \theta^z)}\right) \right]^n \quad (6)$$

and

$$h_0 = A_0 + A_1(\theta - \theta^z) + A_2(\theta - \theta^z)^2 + A_3 \dot{\epsilon}^{cr} + A_4 (\dot{\epsilon}^{cr})^2 \quad (7)$$

The initial deformation is described by:

$$s_0 = S_1 + S_2(\theta - \theta^z) + S_3(\theta - \theta^z)^2 \quad (8)$$

s^* represents the saturation value of s for a given strain rate and temperature. h_0 is the strain hardening or softening constant. \hat{s} is a numerical coefficient, n and a are material parameters The six more parameters that are present in the Abaqus modified Anand model are $A1, A2, A3, A4$ and $S2, S3$.

The Isight optimization flowchart used in the calibration of the material is reported in figure 11 and, for the 3.3 mm thick specimen, also a relaxation test is included. Four different simulations were run simultaneously and the simulation response is compared after each cycle with experimental data. In the optimization component the Neighborhood Cultivation Genetic Algorithm has been used due to his ability to explore all the design space and find a global minimum value of the objective function in case of multi-object optimization. Table 5 synthesizes the parameters obtained as result of the optimization loops and figure 12 illustrates the relative Stress-Strain curves ordered by thickness and strain range.

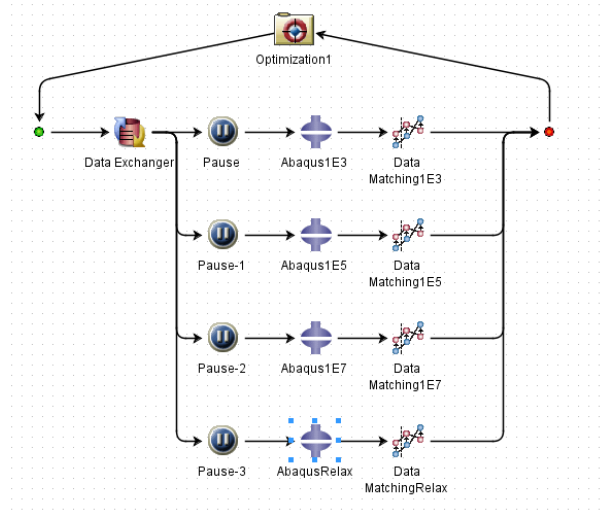


Fig 11. Optimization loop set in Isight for the calibration of the creep constants (top left). Anand creep model compared to experimental results.

Table 5. Anand model constants as fitted for primary and secondary creep.

Parameter	Thickness [mm]	
	1.1 – 1.8	3.3
$S1$	4.8749986	4.2073727
$Q/R [K]$	9599.5582	9845.9687
A	2499.9986	56524.519
ζ	4.5	3.6432953
m	0.41733489	0.43475551
$A0$	153587.88	158793.25
\hat{s}	4.6970472	6.8885417
n	0.037181053	0.011472397
a	2.9462357	2.2818810
$S2$	0	0
$S3$	0	0
$A1$	0	0
$A2$	0	0
$A3$	0	-261661.53
$A4$	0	686840.06

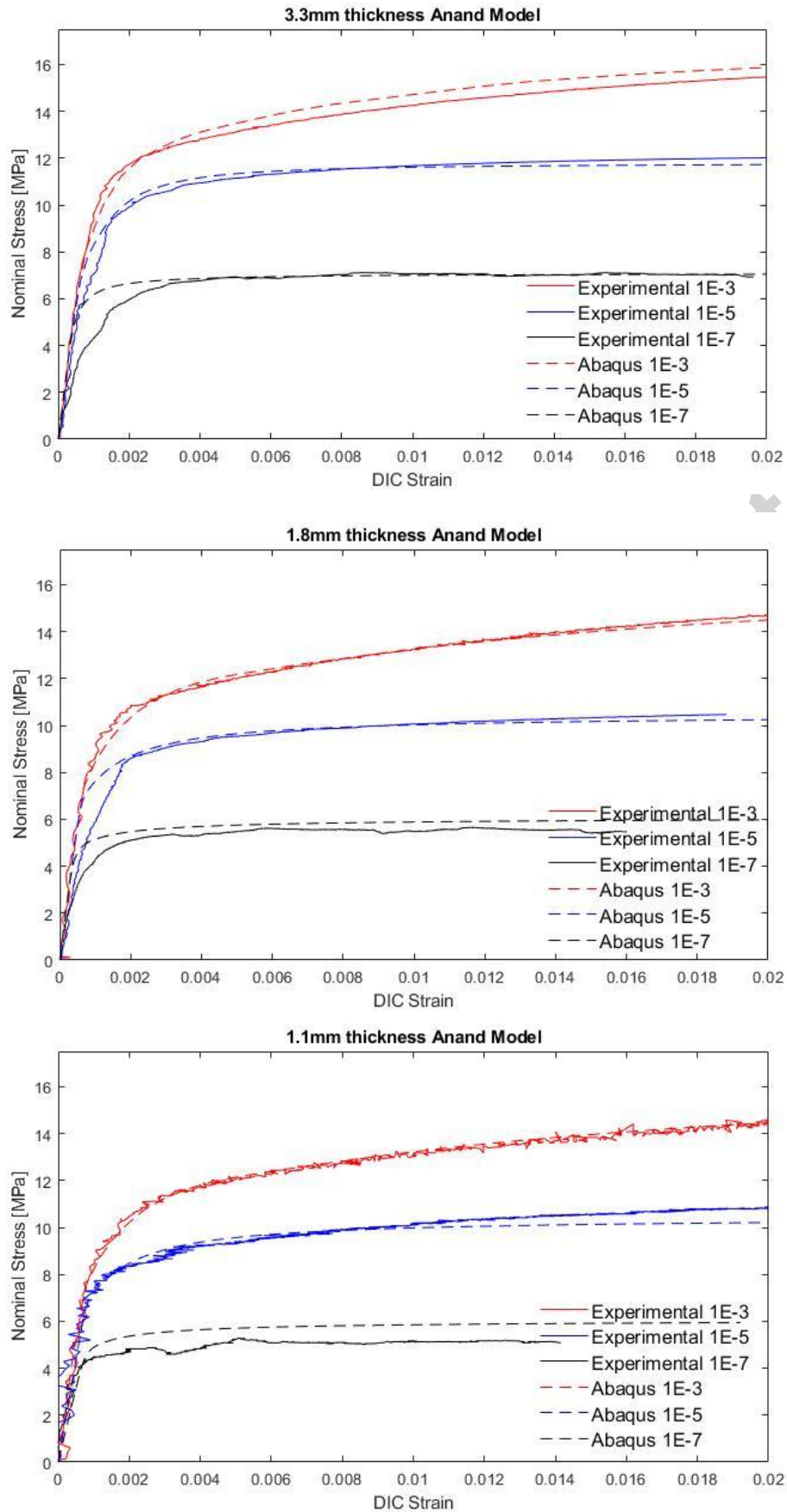


Fig 12. Anand model fitting compared with experimental results for three different strain rates.

Relaxation test

The Isight model was not able to optimize both the tensile and relaxation experiment simultaneously, if this was done considering a perfectly constant global strain during the relaxation phase. By using the parameters obtained from the tensile tests calibration, the numerical stress vs time curve was higher than the one obtained from experimental test. However, the DIC post-processing of the relaxation test showed that, during the hold/relaxation phase, a reduction of strain occurred, most probably due to a slipping in the clamps, figure 13b. By taking into account these effect the FEA simulation gave the correct relaxation behavior.

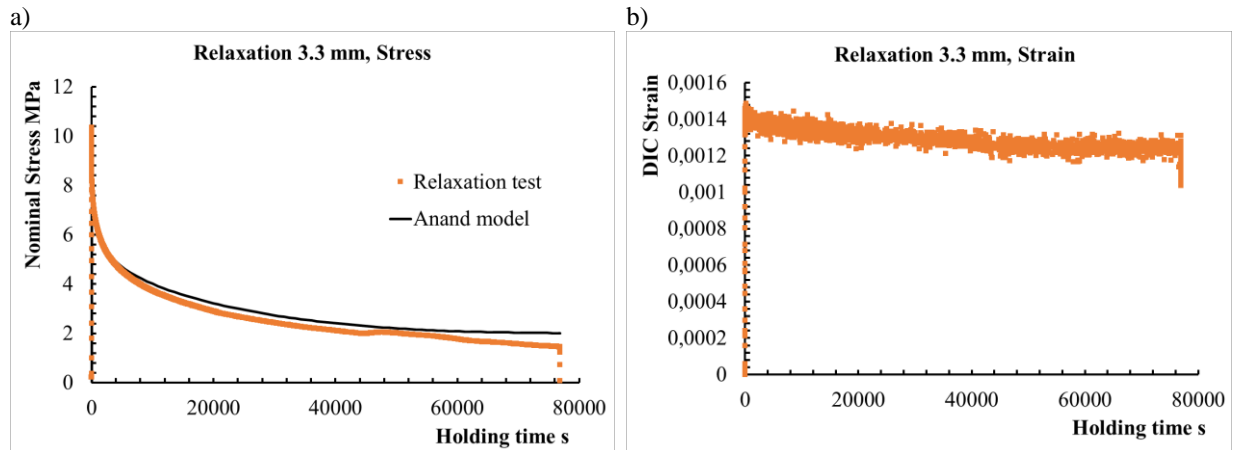


Fig 13. Relaxation test result: Stress vs Time curve (a) and DIC strain vs. time curve (b).

Conclusions

In this study, the behavior of a lead alloy at three different strain rate values was analyzed. Tensile test was conducted on three different geometries, finding a relation between thickness and steady state stress. Based on the test results, two different calibrations were performed, one for the 3.3 mm thick specimen and one suited for the 1.8mm and 1.1mm thick specimens. The derived constitutive laws were implemented in the commercial FEM code Abaqus. Two different models are adopted in this paper. The power law model, most suited for describing the primary creep region, which is attractive for its simplicity. The Anand model, on the other hand, is defined by fifteen parameters and is able to correctly represent also the secondary creep region and the temperature dependent response. Since no temperature dependent test were conducted only the strain rate behavior was calibrated. Isight was used in conjunction with Abaqus for optimizing the model. Due to the highly viscous and non-linear behavior of the material, DIC has been necessary for computing the actual strain values on the specimen's surfaces. In particular, during the relaxation test made on the 3.3 mm thick specimens, a reduction of the longitudinal strain is observed. Considering this trend, the result is in agreement with numerical simulations. For explaining the thickness effect a metallographic investigation has been done, finding bigger average grain size in the 3.3mm specimen. This result explains the different value of steady state stress reached in the experimental test, due to the higher creep resistance for the thicker extrusion. To summarize the main conclusions are:

- The power law creep model is desirable for its simplicity and well performed at the higher strain rates.
- The Anand creep model performed better for the lower strain rates.
- The Anand creep model is indicated also for the time stress response at constant deformation.
- The extrusion thickness resulted proportional to the average grain size, giving an improved resistance for a higher thickness.
- The digital image correlation is an irreplaceable technique when dealing with very ductile alloys.

The present work was financed by Nexans Norway AS and the Research Council of Norway (IPN in ENERGIX Project number 256367) and performed within the project: Next-generation damage based fatigue of cable sheathing (REFACE).

References

- [1] M.E. Kassner, *Fundamentals of Creep in Materials* (Third Edition), Butterworth-Heinemann, 2015, ISBN 9780080994277.
- [2] "H. L. J. Pang, Y. P. Wang, X. Q. Shi and Z. P. Wang, "Sensitivity study of temperature and strain rate dependent properties on solder joint fatigue life," *Proceedings of 2nd Electronics Packaging Technology Conference* (Cat. No.98EX235), 1998, pp. 184-189."
- [3] "Pradeep Lall, Di Zhang, Vikas Yadav, David Locker, High Strain-Rate Constitutive Behavior of SAC105 and SAC305 Leadfree Solder, *IEEE*, 2015".
- [4] M. Motalab, Z. Cai, J. C. Suhling and P. Lall, "Determination of Anand constants for SAC solders using stress-strain or creep data," *13th InterSociety Conference on Thermal and Thermomechanical Phenomena in Electronic Systems*, San Diego, CA, 2012, pp. 910.
- [5] "Farghalli A. Mohamed, Terence G. Langdon, The transition from dislocation climb to viscous glide in creep of solid solution alloys, *Acta Metallurgica*, Volume 22, Issue 6, 1974, Pages 779-788, ISSN 0001-6160".
- [6] "Kassner, M. E. (2000). *Five-power-law creep in single phase metals and alloys*. Oxford: Pergamon."
- [7] "P. Feltham. On the Mechanism of High-Temperature Creep in Metals with Special Reference to Polycrystalline Lead. *Proc Phys Soc.* 69,12-B. 1956".
- [8] "M K Sahota, J R Riddington. Compressive creep properties of lead alloys. *Materials and Design.* 21: 159-167. 2000".
- [9] "DG Harvard. Fatigue of Lead Cable-Sheathing Alloys. Ontario Hydro research. 1972".
- [10] "CW Dollins, CE Betzer. Creep Fracture and Bending of Lead and Lead Alloy Cable Sheathing. *Engineering experiment station bulletin* 440. 1956".
- [11] F. D. W. L. P. Anelli, "The fatigue life of lead alloy E as a sheathing material for submarine power cables.," *Societa' cavi Pirelli*, pp. 86 SM 393-3, 1986.
- [12] "Dassault Systèmes, SIMULIA User Assistance 2017, 2017".
- [13] "Anand, L., "Constitutive Equations for the Rate-Dependent Deformation of Metals at Elevated Temperatures," *Journal of Engineering Materials and Technology*, Vol. 104(1), pp. 12-17, 1982."
- [14] "Brown, S., Kim, K., and Anand, L., "An Internal Variable Constitutive Model for Hot Working of Metals," *International Journal of Plasticity*, Vol. 5(2), pp. 95-130, 1989".
- [15] "Z.N. Cheng, G.Z. Wang, L. Chen, J. Wilde and K. Becker Viscoplastic Anand model for solder alloys and its application *Soldering & Surface Mount Technology* 12/2 [2000] 31±36".
- [16] "Liang Zhang, Ji-guang Han, Yonghuan Guo, Cheng-wen He. 2014. Anand model and FEM analysis of SnAgCuZn leadfree solder joints in wafer level chip scale packaging devices. *Microelectronics Reliability* 54:1, 281-286."
- [17] "B. Rodgers, B. Flood, J. Punch, F. Waldron. Experimental determination and finite element model validation of the anandviscoplasticity model constants for SnAgCu 490-496."
- [18] "Swaminathan, Shriram et al. "Calibrating Material Constants from Experimental Data for Lead-free Solder Materials Using a Parametric Optimization Approach." (2011)."
- [19] "Garofalo, F., 1963. An empirical relation defining the stress dependence of minimum creep rate in metals *Trans. Metall. Soc. AIME*, 227 (1963), pp. 351-356".